RSC Advances

ROYAL SOCIETY OF CHEMISTRY

www.rsc.org/advances

Graphical Abstract

A new promising sensor for detecting methanol has been prepared, which exhibits highly sensitive and selective luminescence quenching to methanol.

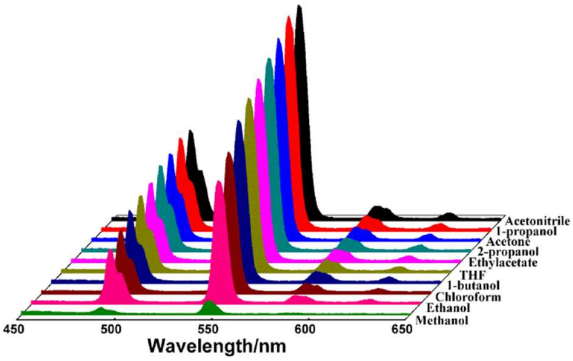

Cite this: DOI: 10.1039/c0xx00000x

www.rsc.org/xxxxxx

PAPER

A luminescent terbium coordination polymer for sensing methanol†

Hong-Ming Wang,[a,b] Huiping Liu,[a] Tian-Shu Chu,[a] Yang-Yi Yang,*[a] Yun-Song Hu,[a] Seik Weng Ng[c,d] and Wen-Ting Liu[a,b]

Received (in XXX, XXX) Xth XXXXXXXXX 20XX, Accepted Xth XXXXXXXXX 20XX

DOI: 10.1039/b000000x

Two isostructural one-dimensional lanthanide coordination polymers, with the general formula $\{[Ln(aip)(H_2O)_5]\cdot 0.5(bdc)\cdot 3H_2O\}_n$ [Ln = Eu (**1**), Tb (**2**); H_2aip = 5-aminoisophthalic acid, H_2bdc =1,4-benzenedicarboxylic acid), have been synthesized by diffusion technique at room temperature. Their structures were identified by X-ray diffraction. Complex **2** exhibits green emission, corresponding to the $^5D_4 \rightarrow {}^7F_J$ (J = 6–3) transitions of Tb^{3+} ion. Significantly, when **2** was immersed in different organic solvents, it had a unique response to methanol compared to other solvents. Furthermore, **2** displayed highly sensitive and selective luminescence quenching to methanol with the ignorable interference of other small-molecule organics. This makes it a potential luminescence sensor for actual application in recognizing methanol.

Introduction

Lanthanide coordination polymers (Ln-CPs), which are constructed from lanthanide ions as nodes and organic ligands as linkers, have received considerable attention in the past few years not only because of their intriguing varieties of architectures and topologies but also owing to their wide range of potential applications in luminescence,[1-4] gas storage and separation,[5] magnetism,[6] catalysis[7] *etc*. Ln-CPs possess lots of fascinating photophysical properties arising from f-f transitions *via* suitable "antenna effect",[8] such as larger Stokes shifts, narrow line emission, relatively long luminescence lifetimes and high color purity,[9] which make them particularly attractive for applications in phosphorescent probes and luminescence bioassays.[10] However, among numerous lanthanide-derived CPs that have been synthesized up to now, only a few of them, which have a specific and detectible change in luminescence when in contact with target analyte, have potential application as chemical sensors.[11] Taking advantage of the optical properties of lanthanide ion, more and more lanthanide-based sensors, such as sensing anions,[12, 13] cations,[14, 15] small organic molecules[16-18] and temperature,[19, 20] have been realized and reported up till now. Meanwhile, such advancement also guides and encourages us to rationally design and synthesize more characteristic Ln-CPs for the individual recognition of analytes *via* appropriate choice of organic ligand.

At present, aromatic polycarboxylic acids are the most commonly employed ligands binding to the lanthanide ions because they are good agents as antenna[21] to promote luminescence by effective energy transfer and have versatile coordination modes.[22] Adding the auxiliary ligands in the synthesis of Ln-CPs may result in new structure types as well as bring interesting properties.[23] Keeping the above in mind, we selected 5-aminoisophthalic acid and 1,4-benzenedicarboxylic acid as mixed ligands to construct Ln-CPs based on the following considerations: (i) the amino group of 5-aminoisophthalic acid can act as the hydrogen-bond acceptor or donor to form rich hydrogen bonds with the neighboring moieties, which is often useful for the formation of stable supramolecular structure;[24] (ii) the amino group, as an electron-donating group, increases the electron density of the ligand and consequently may affect luminescence intensities of the lanthanide coordination polymers;[25] (iii) terephthalic acid exhibits rigidity, highly chemical and thermal stabilities, which have been proven to be beneficial to enhance the robustness of the resulting coordination polymers.[26]

Methanol can cause severe health problems to human beings when it is ingested or inhaled due to its high toxicity. The excessive exposure of the body to methanol usually leads to headache, vertigo, fatigue, nausea, vomiting, blurred vision, blindness and even death.[27] But as a cheaper and more easily accessible raw material, methanol is widely used in many fields despite the poisonousness. For example, the manufacturing of herbal medicine usually uses methanol as a solvent to extract natural ingredients.[28] Therefore, for consumer protection, it is

[a]*MOE Key Laboratory of Bioinorganic and Synthetic Chemistry, KLGHEI of Environment and Energy Chemistry, School of Chemistry and Chemical Engineering, Sun Yat-Sen University, Guangzhou, 510275, P. R. China. E-mail: cesyyy@mail.sysu.edu.cn*

[b]*Department of Chemistry, Guangdong University of Education, Guangzhou, 510303, P. R. China*

[c]*Department of Chemistry, University of Malaya,50603 Kuala Lumpur, Malaysia*

[d]*Department of Chemistry, Faculty of Science, King Abdulaziz University, Jeddah, Saudi Arabia*

†Electronic Supplementary Information (ESI) available: Experimental details and supplementary figures. CCDC 979520. For ESI and crystallographic data in CIF see DOI: 10.1039/b000000x/

imperative to detect the content of methanol. The determination of methanol is mainly carried out by instrumental methods, such as high performance gas chromatography (GC),[27] gas chromatography and mass spectrometry (GC/MS).[29] Although the techniques have been demonstrated to be highly sensitive, the high cost of the equipment and the complication of the sample preparation limit their wide application in daily life.[11] Sensor technology is much simpler in instrumental implementation and sample preparation. Increasing interest was found in the recognition and sensing small molecules using Ln-CPs as optical probes for their important roles in biological and environmental systems.[30] Methanol is expected to decrease the luminescence intensities of Ln-CPs in the coordination environment or in close proximity to the emitting lanthanide ion because of its high-vibrational frequency.[31]

As part of our ongoing efforts in the design and synthesis of functional materials, we have reported some luminescent Ln-CPs and their sensing applications.[32-34] Herein, two Ln-CPs based on H_2aip and H_2bdc mixed ligands were prepared under mild conditions, namely, $\{[Ln(aip)(H_2O)_5]\cdot 0.5(bdc)\cdot 3H_2O\}v_n$ (Ln = Eu for **1** and Tb for **2**). The structure of **1** was determined by single-crystal X-ray diffraction analysis. The structure of **2** was identified and characterized by powder X-ray diffraction (PXRD) studies. The thermal stability and photoluminescence properties have been examined. Significantly, the luminescent response of **2** as a highly selective phosphorescent probe for methanol was further investigated in detail. It is very exciting that the luminescent response was not obviously influenced by the presence of other solvents.

Experimental

General procedures

All chemicals were commercially available and used without further purification.

Synthesis of $\{[Eu\ (aip)(H_2O)_5]\cdot 0.5(bdc)\cdot 3H_2O\}_n$ (1)

8 mL of an ethanolic solution of $EuCl_3\cdot 6H_2O$ (0.0367 g, 0.10 mmol) was carefully layered on a 10 mL aqueous solution of H_2aip (0.0145 g, 0.08 mmol), H_2bdc (0.0133 g, 0.08 mmol) and NaOH (0.0128 g, 0.32 mmol) in a long test tube, which was sealed with plastic wrap. The solution was left to stand for 6 weeks at room temperature, and gray crystals of **1** (yield: 56%, based on Eu^{3+}) were obtained. Elemental analysis calcd (%) $C_{12}H_{23}NO_{14}Eu$: C, 25.84; H, 4.13; N, 2.51. Found (%): C, 25.69; H, 4.02; N, 2.43. IR (KBr, cm^{-1}): 3351s, 1543s, 1479w, 1453w, 1399s, 750m.

Synthesis of $\{[Tb\ (aip)(H_2O)_5]\cdot 0.5(bdc)\cdot 3H_2O\}_n$ (2)

2 was prepared in the same way as **1** but using $TbCl_3\cdot 6H_2O$ (0.0373 g, 0.10 mmol) instead of $EuCl_3\cdot 6H_2O$. Gray crystals of **2** (yield: 61%, based on Tb^{3+}) were obtained after 6 weeks. Elemental analysis calcd (%) $C_{12}H_{23}NO_{14}Tb$: C, 25.52; H, 4.08; N, 2.48. Found (%): C, 25.41; H, 4.01; N, 2.39. IR (KBr, cm^{-1}):3349s, 1543s, 1482w, 1457w, 1401s, 751m.

Physical measurements

Single crystal X-ray diffraction data were collected at 100 K on a Bruker Smart 1000 CCD diffractometer, using graphite monochromatized Mo Kα radiation (λ = 0.71073Å). The structure was solved with direct methods (SHELXS) and then refined with full matrix least-squares method against F_o^2 using the SHELXTL software.[35, 36] Details of the crystal parameters data collection and refinement for **1** are summarized in Table S1 (see ESI†). Selected bond distances and angles are listed in Table S2 in the Supporting information. Other measurements were carried out at room temperature. C, H, and N microanalyses were carried out with an Elementar Vario EL elemental analyzer. FT-IR spectra were recorded from KBr pellets in the range of 4000–400 cm^{-1} on a Nicolet 330 FT-IR spectrometer. Thermogravimetric (TG) analysis experiment was performed on a Netzsch TG-209 instrument from room temperature to 800 °C at a heating rate of 10 °C min^{-1} under an ambient atmosphere. The powder X-ray diffraction patterns were recorded on a D/MAX 2200VPC diffractometer with Cu- Kα radiation (λ = 1.5409 Å) at a scanning rate of 5° min^{-1} with 2θ ranging from 5 to 50°c. Luminescence spectra were collected by a RF-5301PC luminescence spectrometer. Samples that were used for luminescence measurements were examined by PXRD to ensure that they were in the pure phase. Fluorescence lifetimes were obtained by a combined fluorescence lifetime and steady-state spectrometer (FLSP920, Edinburgh) with a μF900 xenon lamp.

Results and discussion

Synthesis and characterization

The structure of **1** was determined by single-crystal X-ray diffraction. However, the crystal quality of **2** was too poor to measure by X-ray diffraction, even though we have made many attempts to do so. Fortunately, the PXRD pattern of the as-synthesized sample of **2** was closely matched to the simulated XRD pattern generated from the single-crystal structure of **1** (Fig. S1), which suggests that complexes **1** and **2** are isostructural.[37] Both complexes are stable and insoluble in common organic solvents and water.

The IR spectra show features attributable to each component of the complexes. As shown in Fig. S2, the absorption bands at 1693 cm^{-1} and at 1682 cm^{-1} correspond to the asymmetric stretching vibration of carbonyl groups in H_2aip and H_2bdc, respectively. The absence of characteristic peaks at around 1700 cm^{-1} indicates the complete deprotonation of carboxyl for the ligands in complexes,[38] which is in good agreement with the solid state structural feature. Moreover, the IR spectra of **1** and **2** exhibit broad absorption bands centred at *ca.* 3350 cm^{-1} which are typical of the O–H stretching vibration of water, thereby confirming the presence of water molecules in the coordination spheres of the complexes.

The thermal stability of complex **2** was examined in air by thermogravimetric analysis (TGA). As indicated in Fig. S3, **2** shows a rapid weight loss of 9.84% between 20 and 100 °C, corresponding to the loss of three guest water molecules (calculated 9.57%). The sample maintains unchanged in the temperature range from 145 to 380 °C. Above 380 °C, the removal of five coordinated water molecules occurs and is accompanied by the decomposition of ligands and the collapse of structure. The remaining weight of 35.34% corresponds to terbium oxide Tb_4O_7 (calculated: 33.13%). These results suggest

that the complex **2** is stable in air below 380 °C.

Crystal structure of $\{[Eu(aip)(H_2O)_5]\cdot 0.5(bdc)\cdot 3H_2O\}_n$

Complex **1** crystallizes in monoclinic system, $P2_1/c$ space group. The asymmetric unit contains one crystallographically independent Eu^{3+} ion, one aip ligand, five coordinated water molecules, half bdc ligand and three free water molecules. As shown in Fig. 1a, each Eu^{3+} ion is nine-coordinated by four

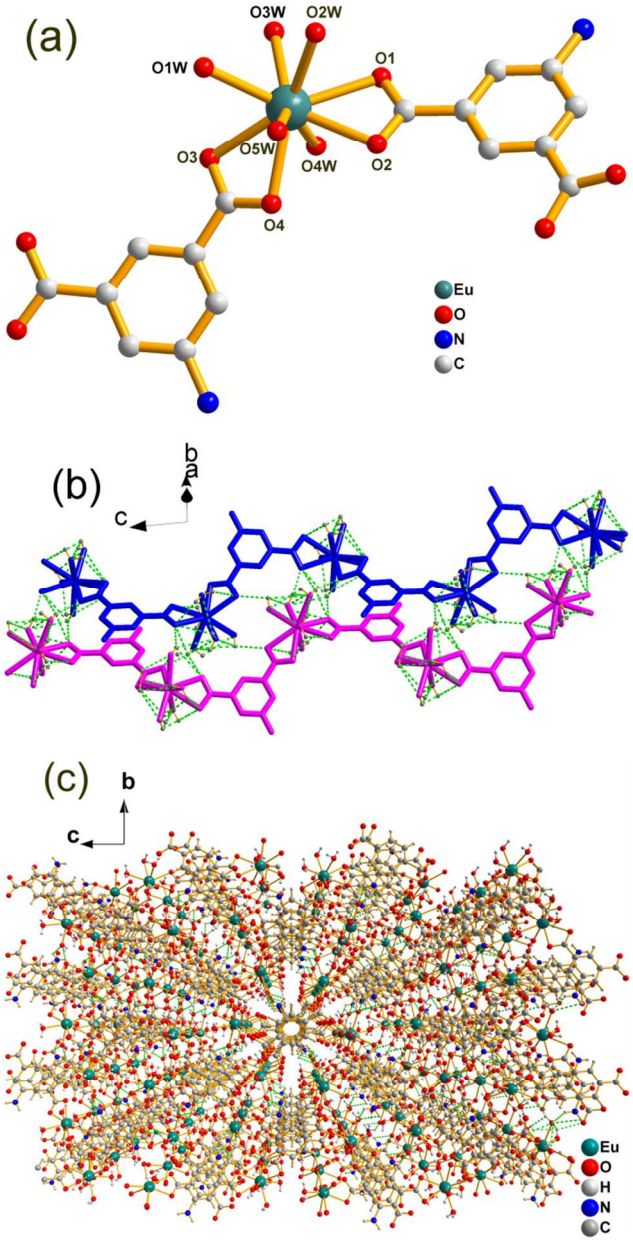

Fig. 1 (a) The coordination environment of the Eu^{3+} in **1**; (b) perspective view of the double chains in the *bc* plane. For clarity, uncoordinated terephthalate ligands and water molecules have been omitted; (c) 3D supramolecular network of **1** viewed along the *a* axis. Hydrogen bonds are shown as a green dashed line.

oxygen atoms from two aip ligands and five oxygen atoms from five water molecules, forming a slightly distorted tricapped trigonal prism geometry (Fig. S4). The Eu – O distance is in the range of 2.361(6) – 2.546(6) Å, and the coordination bond angles around the Eu^{3+} ion vary from 52.2(2)° to 145.9(2)°, all of which are within the normal range.[39] All the two carboxylate groups of the H_2aip ligand are deprotonated, and coordinate to different Eu^{3+} ions with bidentate-chelating mode (Fig. S5). Thus, every aip ligand in a bisbidentate manner is linked to two adjacent Eu^{3+} ions with Eu···Eu separation of 9.8271(6) Å, resulting in a 1D zigzag chain-like structure in the *bc* plane. As shown in Fig. 1b, the coordination between the Eu^{3+} ions and aip ligands affords the juxtaposition of double chains with the chemical formula $[Eu(aip)(H_2O)_5]$. The two chains interact with each other through hydrogen bonds and π-π stacking between the aromatic rings of aminoisophthalate ligands that belong to adjacent chains. The guest water molecules and bdc ligands fill between the double-chain molecular motifs (Fig. S6). Although the carboxylate oxygen atoms from bdc ligands are uncoordinated to the Eu^{3+} ion, they form hydrogen bonds with the coordinated water molecule (O4w–H4w1··· O5: 2.56 Å, 113°; O4w–H4w2··· O6: 2.30 Å, 137°) and the uncoordinated water molecule (O8w–H8w2··· O5: 2.23 Å, 130°; O8w–H8w1··· O6: 2.00 Å, 153°). In addition, the lattice water molecules serve both as hydrogen bond donors (O6w–H6w1 ··· O6: 1.95 Å, 172°; O6w–H6w2 ··· O7w: 2.08 Å, 149°) and acceptors (O2w–H2w1··· O6w: 2.10 Å, 141°). Through the connections of extensive hydrogen bonds (Table S3), the chains are further stacked to a 3D supramolecular network along the *a* axis (Fig. 1c).

Photoluminescence properties

The excitation and emission spectra of **2** were recorded at room temperature. As revealed in Fig. 2a, the excitation spectra show broad bands in the range of 270–385 nm, which are ascribed to the π–π* electron transition of the organic ligands. The maximal band in the excitation spectrum of **2** in solid state is 354 nm, whereas that in acetonitrile is 341 nm. The excitation spectrum of **2** in solid state is slightly red-shifted relative to that in acetonitrile. The emission spectra of **2** both in solid state and in acetonitrile have identical profile (Fig. 2b) due to the f-f transitions of Tb^{3+} ions. A series of characteristically narrow emission bands that are centered at 490, 546, 586, and 624 nm can be assigned to transitions of the $^5D_4$ excited state to the corresponding ground state ^7F_J (J =6–3) of Tb^{3+}. The most intense emission at 546 nm is attributed to the $^5D_4 \rightarrow {}^7F_5$ transition, which is hypersensitive to the coordination environment of Tb^{3+} ion and implies a green emission light. The medium-strong emission at 490 nm corresponds to the $^5D_4 \rightarrow {}^7F_6$ transition, which is fairly insensitive to the environment of Tb^{3+} ion.[40] The intensity of the $^5D_4 \rightarrow {}^7F_5$ transition is stronger than that of the $^5D_4 \rightarrow {}^7F_6$ transition, implying that the Tb^{3+} ion is not located at the inversion centre and the symmetry of Tb^{3+} ion site is low. The luminescence lifetimes were obtained from the decay curves by fitting them with biexponential functions (Fig. S7, Supporting information), indicating the presence of two emissive Tb^{3+} centers in the complex.[41] The luminescence lifetime at 546 nm ($^5D_4 \rightarrow {}^7F_5$) of **2** in solid state [τ_1 = 0.111 ms (39.10%) and τ_2 = 0.329 ms (60.90%)] is shorter than that in acetonitrile [τ_1 = 0.145 ms (9.53%) and τ_2 = 0.406 ms (90.47%)].

At the beginning, the emission spectrum of **1** was measured in the same condition as **2**, i.e., the excitation and emission slits were 3/3 nm. Unexpectedly, neither the characteristic emission bands of Eu^{3+} nor the fluorescence of ligands could be observed

(Fig. S8). Nevertheless, when the excitation and emission slits were 10/10 nm, the emission bands for Eu^{3+} at 592 and 616 nm could be observed, which are ascribed to the $^5D_0 \rightarrow {}^7F_1$ and $^5D_0 \rightarrow {}^7F_2$ transitions, respectively. At the same time, the fluorescence of ligands was detected in the 395-510 nm region (Fig. S8), indicating that the energy transfer from the organic ligands to Eu^{3+} ions is not efficient,[42] due to the poor match of the triplet energy levels of the ligands with that of the emitting level of the central Eu^{3+} ions.[43] In contrast, for complex 2, Tb^{3+}-centred luminescence could be observed, whereas the ligand-based fluorescence disappeared (Fig. S9), indicating such energy transfer is very efficient. The above results suggest that 5-aminoisophthalic acid is a poor sensitizer for Eu^{3+} and a good antenna ligand for Tb^{3+}.

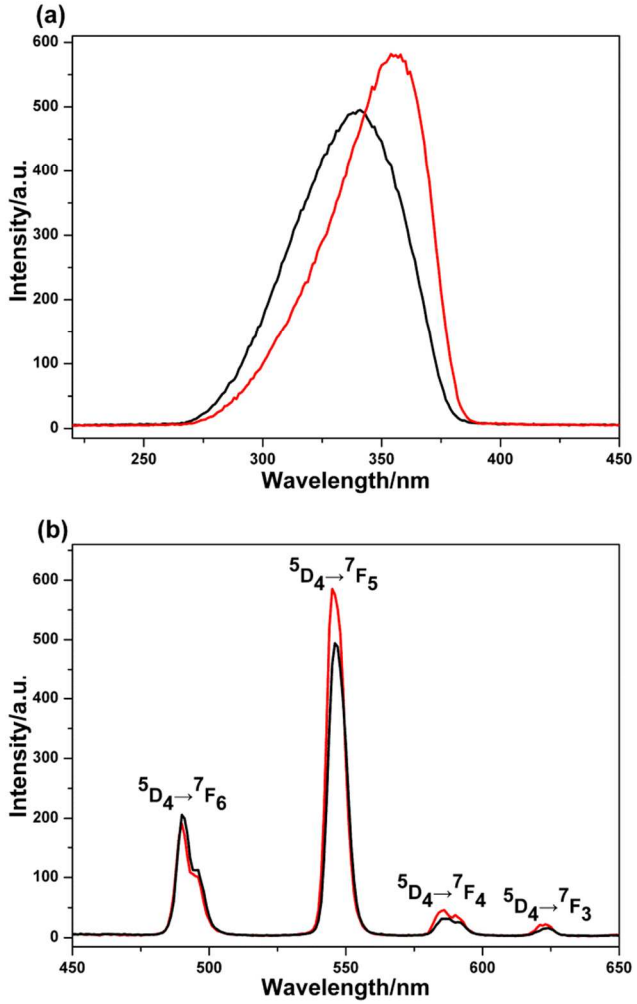

Fig. 2 (a) Excitation spectra of **2** both in solid state (red) and in acetonitrile (black), monitored at 546 nm; (b) emission spectra of **2** both in solid state (red) and in acetonitrile (black), excited at 354 nm and 341nm, respectively.

Selective sensing for methanol

In order to examine the potential of **2** for small molecule recognition**,** the powdery sample of **2** was immersed in methanol, ethanol, 1-propanol, 2-propanol, 1-butanol, acetone, acetonitrile, chloroform, ethylacetate and tetrahydrofuran (THF) solvent**s** for luminescence experiments upon excitation at 341 nm. The photoluminescence response of **2** for the various organic molecules is shown in Fig. 3. The histogram (Fig. 4) clearly shows that the luminescent intensities of $^5D_4 \rightarrow {}^7F_5$ transition of Tb^{3+} ions are strongly dependent on the identity of the solvent molecules, especially in the case of methanol, which exhibited the most noticeable quenching effect. Such solvent-dependent luminescence properties are very interesting and significant for the sensing methanol solvent molecules. Therefore, the influence of methanol on the luminescent intensity of **2** has been explored in more detail.

2 was dispersed in acetonitrile as the standard suspension, while the content of methanol was gradually increased to detect the emissive response. As shown in Fig. 5, the luminescent intensity of the suspension remarkably decreased with the addition of methanol, and it almost disappeared at a methanol content of 7.0 vol%. Furthermore, the decreasing trend of the $^5D_4 \rightarrow {}^7F_5$ transition intensity of Tb^{3+} at 546 nm *versus* the volume ratio of methanol could be well fitted with a first-order exponential decay (Fig. S10), which indicated that luminescence quenching of **2** by methanol is diffusion-controlled.[9, 30, 44]

Inspired by the results above, the sensing sensitivity towards methanol was further investigated. As shown in Fig. 6, when the additional amount of methanol was 7.0 vol%, the luminescent intensity of **2** in acetonitrile at 546 nm was decreased by 94% of

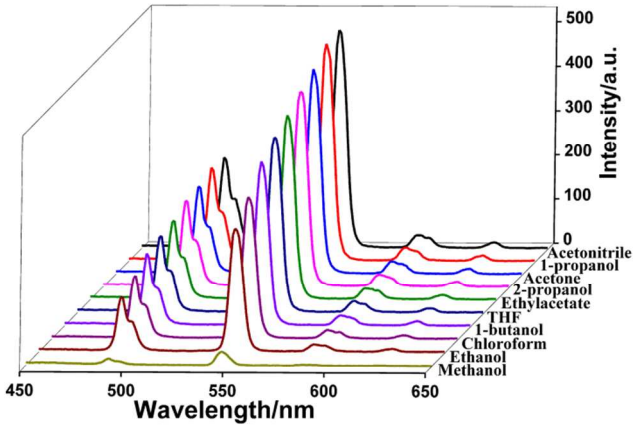

Fig. 3 Room-temperature emission spectra of **2** dispersed into different solvents at an excitation of 341 nm.

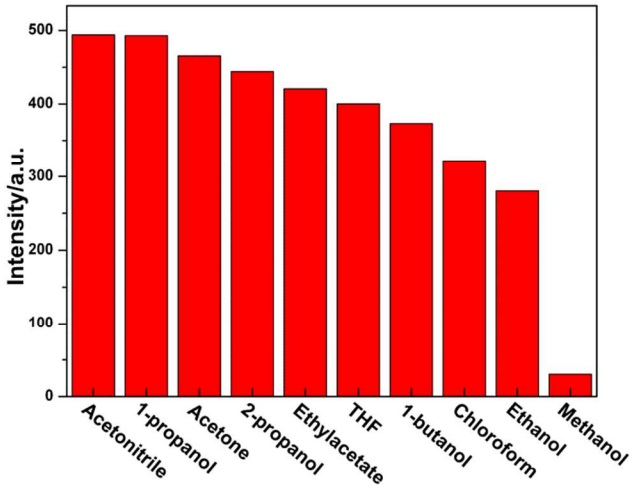

Fig. 4 Diagrams of the $^5D_4 \rightarrow {}^7F_5$ transition intensities of **2** at 546 nm in different solvents when excited at 341 nm.

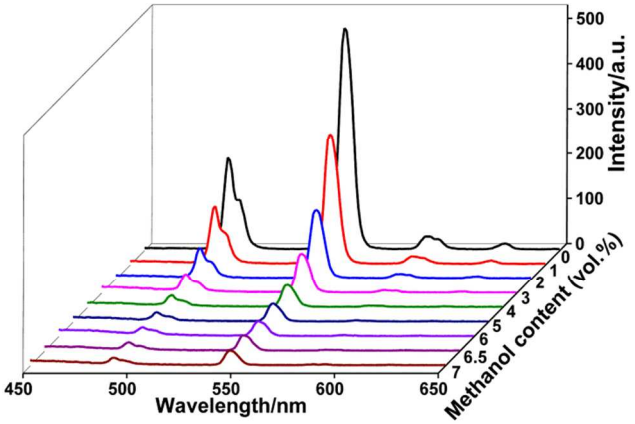

Fig. 5 The PL spectra of **2**/acetonitrile emulsion in the presence of various amounts of methanol upon excitation at 341 nm.

its initial value. In contrast, other organic solvents have a negligible effect on the luminescence intensity of **2**. In addition, competitive experiment was carried out by adding methanol to the acetonitrile suspension in the presence of other organic compound. As shown in Fig. 7, the phosphorescent response of **2** to methanol was nearly undisturbed by other organics. It is worth mentioning that the sensing function of **2** for methanol showed almost no obvious change even when many organics coexisted in the acetonitrile suspension (Fig. S11 and Fig. S12). The results suggest that **2** is a promising luminescent chemosensor for methanol with high sensitivity and selectivity.

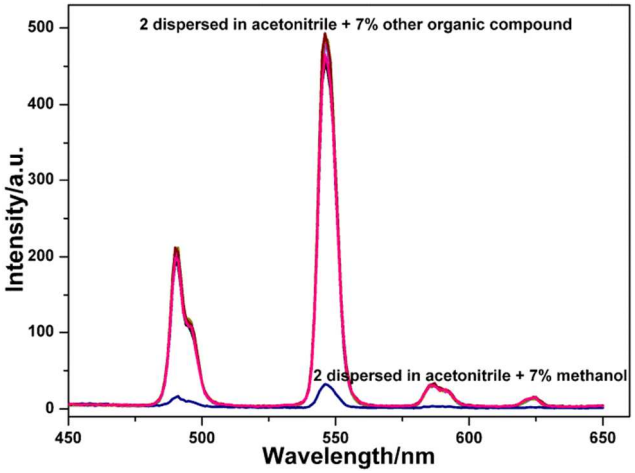

Fig. 6 Emission spectra of **2** introduced into acetonitrile on the addition of different solvents.

To explain the possible sensing mechanism exhibited by the complex **2** toward methanol as well as to confirm if the structure of **2** collapses or remains in the presence of methanol, solid sample was obtained by filtration of the emulsion of **2** in acetonitrile and 7% methanol, washing with water, and drying in air. The PXRD pattern of the solid sample matches well with that of as-synthesized **2** (Fig. S1), indicating that the structure of **2** remains unchanged after solvent immersion.

It is well established that the luminescent intensity of lanthanide ion (Ln^{3+}) relies on the efficiency of energy transfer from the ligand to Ln^{3+} center.[45, 46] However, the mechanism for such significant quenching effects of small molecule solvents has not been very clear up to now. Nevertheless, the influence of

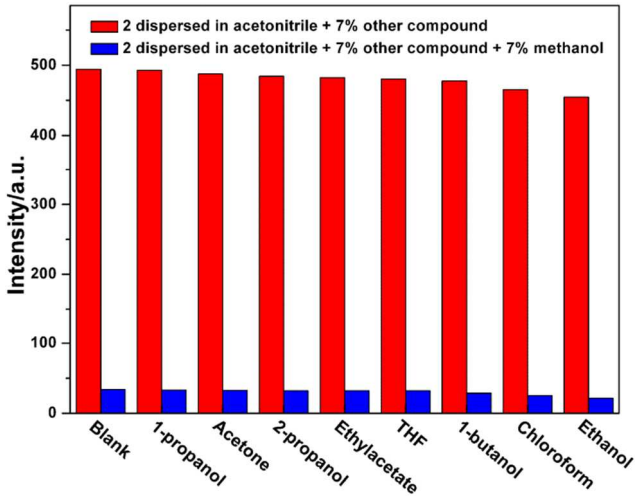

Fig. 7 The $^5D_4 \rightarrow {}^7F_5$ transition intensities of **2** dispersed into acetonitrile on the addition of different organics (red) and subsequent addition of methanol (blue) when excited at 341 nm.

guest solvents on the ligand–metal energy transfer efficiency definitely plays an important role.[47] As for the reason of the quenching by methanol, it is reasonable to suggest that the interaction of methanol molecules with the open metal sites or the ligands may hinder the energy transfer from the ligand to Tb^{3+}. Additionally, the vibration-induced deactivation of methanol can also reduce the energy transfer, thus dramatically quenching the luminescence of Tb^{3+} in **2**. The quenching mechanism is similar to that proposed in the previous literature.[44, 47, 48] More investigations are required to explore the mechanism in depth in order to rationally design and construct various sensing materials of lanthanide coordination polymers for different analytes detection.

Conclusions

In conclusion, two new isostructural lanthanide coordination polymers have been successfully designed and synthesized by phase diffusion method under mild condition. They possess 1D double zigzag chains that are further connected by hydrogen bonds to assemble 3D supramolecular structures. The complex **1** displays weak emission due to the poor match of the triplet energy levels of ligands with that of $^5D_0$ of level Eu^{3+}, whereas complex **2** exhibits strong characteristic emission peaks of Tb^{3+}. **2** showed a significant quenching effect in the luminescence emission of Tb^{3+} upon the introduction of methanol. Moreover, no obvious interference from other organic solvents such as ethanol, 1-propanol, 2-propanol, 1-butanol, acetone, acetonitrile, chloroform, ethylacetate and THF was observed. The results indicate that **2** could be a promising sensor for recognizing methanol with excellent selectivity and sensitivity, which makes it a potential candidate for monitoring methanol in biological and environmental areas, and further research on this subject is currently under way.

Acknowledgements

The authors acknowledge the financial support of the National Natural Science Foundation of China (20973203 and 91022012) and the Fundamental Research Funds for the Central Universities.

References

1 L. Armelao, G. Bottaro, S. Quici, M. Cavazzini, C. Scalera and G. Accorsi, *Dalton Trans*., 2011, **40**, 11530-11538.

2 S. Deslandes, C. Galaup, R. Poole, B. Mestre-Voegtle, S. Soldevila, N. Leygue, H. Bazin, L. Lamarque and C. Picard, *Org. Biomol. Chem.*, 2012, **10**, 8509-8523.

3 H. B. Xu, J. G. Deng and B. Kang, *RSC Adv.*, 2013, **3**, 11367-11384.

4 Y. M. Zhu, M. Y. Xie, R. Zhang, Y. Y. Yang, C. H. Zeng, F. L. Zhao, Y. X. Tong, C. Y. Su and W. T. Wong, *Photochem. Photobiol. Sci.*, 2011, **10**, 1760-1765.

5 H. He, H. Ma, D. Sun, L. Zhang, R. Wang and D. Sun, *Cryst. Growth Des.*, 2013, **13**, 3154-3161.

6 D. K. Cao, Y. H. Zhang, J. Huang, B. Liu and L. M. Zheng, *RSC Adv.*, 2012, **2**, 6680-6685.

7 Y. H. Zheng, J. T. Lin and Q. M. Wang, *Photochem. Photobiol. Sci.*, 2012, **11**, 1567-1574.

8 A. Bourdolle, M. Allali, J. C. Mulatier, B. Le Guennic, J. M. Zwier, P. L. Baldeck, J. C. G. Bunzli, C. Andraud, L. Lamarque and O. Maury, *Inorg. Chem.*, 2011, **50**, 4987-4999.

9 Z. Hao, X. Song, M. Zhu, X. Meng, S. Zhao, S. Su, W. Yang, S. Song and H. Zhang, *J. Mater. Chem. A*, 2013, **1**, 11043-11050.

10 P. Horcajada, R. Gref, T. Baati, P. K. Allan, G. Maurin, P. Couvreur, G. Ferey, R. E. Morris and C. Serre, *Chem. Rev.*, 2012, **112**, 1232-1268.

11 Z. Jin, H. He, H. Zhao, T. Borjigin, F. Sun, D. Zhang and G. Zhu, *Dalton Trans.*, 2013, **42**, 13335-13338.

12 C. L. Tan and Q. M. Wang, *Inorg. Chem.*, 2011, **50**, 2953-2956.

13 K. L. Wong, G. L. Law, Y. Y. Yang and W. T. Wong, *Adv. Mater.*, 2006, **18**, 1051-1054.

14 B. L. Chen, L. B. Wang, Y. Q. Xiao, F. R. Fronczek, M. Xue, Y. J. Cui and G. D. Qian, *Angew. Chem. Int. Ed.*, 2009, **48**, 500-503.

15 L. Zhao, Y. Liu, C. He, J. Wang and C. Duan, *Dalton Trans.*, 2014, **43**, 335-343.

16 X. J. Zhao, J. H. Yang, Y. Liu, P. F. Gao and Y. F. Li, *RSC Adv.*, 2014, **4**, 2573-2576.

17 Z. Zhou, C. L. Tan, Y. H. Zheng and Q. M. Wang, *Sens. Actuators, B*, 2013, **188**, 1176-1182.

18 Y. Li, S. Zhang and D. Song, *Angew. Chem. Int. Ed.*, 2013, **52**, 710-713.

19 X. Rao, T. Song, J. Gao, Y. Cui, Y. Yang, C. Wu, B. Chen and G. Qian, *J. Am. Chem. Soc.*, 2013, **135**, 15559-15564.

20 K. Miyata, Y. Konno, T. Nakanishi, A. Kobayashi, M. Kato, K. Fushimi and Y. Hasegawa, *Angew. Chem. Int. Ed.*, 2013, **52**, 6413-6416.

21 L. Armelao, S. Quici, F. Barigelletti, G. Accorsi, G. Bottaro, M. Cavazzini and E. Tondello, *Coord. Chem. Rev.*, 2010, **254**, 487-505.

22 G. L. Law, K. L. Wong, Y. Y. Yang, Q. Y. Yi, G. Jia, W. T. Wong and P. A. Tanner, *Inorg. Chem.*, 2007, **46**, 9754-9759.

23 S. Chen, R. Q. Fan, C. F. Sun, P. Wang, Y. L. Yang, Q. Su and Y. Mu, *Cryst. Growth Des.*, 2012, **12**, 1337-1346.

24 H. G. Jin, Y. Z. Yan, J. Li, Z. G. Gu, J. H. Chen, Y. T. Liu, Z. P. Zheng, Q. G. Zhan and Y. P. Cai, *Inorg. Chem. Commun.*, 2012, **23**, 25-30.

25 S. Sivakumar, M. L. Reddy, A. H. Cowley and K. V. Vasudevan, *Dalton Trans.*, 2010, **39**, 776-786.

26 M. E. Theresa M. Reineke, M. OKeeffe, and Omar M. Yaghi, *Angew. Chem. Int. Ed.*, 1999, **38**, 2590-2594.

27 M. L. Wang, J. T. Wang and Y. M. Choong, *J. Food Compos. Anal.*, 2004, **17**, 187-196.

28 C. C. Kuo, Y. H. Wen, C. M. Huang, H. L. Wu and S. S. Wu, *J. Food Drug Anal.*, 2002, **10**, 101-106.

29 X. Xu, J. Fillos, K. Ramalingam and A. Rosenthal, *Anal. Methods*, 2012, **4**, 3688-3694.

30 J. M. Zhou, W. Shi, N. Xu and P. Cheng, *Inorg. Chem.*, 2013, **52**, 8082-8090.

31 S. Sivakumar and M. L. P. Reddy, *J. Mater. Chem.*, 2012, **22**, 10852.

32 C. H. Zeng, Y. Y. Yang, Y. M. Zhu, H. M. Wang, T. S. Chu and S. W. Ng, *Photochem. Photobiol.*, 2012, **88**, 860-866.

33 H. M. Wang, Y. Y. Yang, C. H. Zeng, T. S. Chu, Y. M. Zhu and S. W. Ng, *Photochem. Photobiol. Sci.*, 2013, **12**, 1700-1706.

34 Y. M. Zhu, C. H. Zeng, T. S. Chu, H. M. Wang, Y. Y. Yang, Y. X. Tong, C.-Y. Su and W. T. Wong, *J. Mater. Chem. A,* , 2013, 11312 – 11319.

35 G. M. Sheldrick, *SHELXS-97, Program for Cryatal Structure Solution*, University of Göttingen, Göttingen, Germany, 1997.

36 G. M. Sheldrick, *SHELXL-97, Program for Crystal Structure Refinement*, University of Göttingen, Göttingen, Germany, 1997,.

37 J. J. Wu, Y. X. Ye, Y. Y. Qiu, Z. P. Qiao, M. L. Cao and B. H. Ye, *Inorg. Chem.*, 2013, **52**, 6450-6456.

38 S.-M. Fang, M. Hu, L.-R. Jia, C. Wang, Q. Zhang, S.-T. Ma, M. Du and C.-S. Liu, *CrystEngComm*, 2011, **13**, 6555-6563.

39 Y. Luo, G. Calvez, S. Freslon, K. Bernot, C. Daiguebonne and O. Guillou, *Eur. J. Inorg. Chem.*, 2011, 3705-3716.

40 X. Ma, X. Li, Y. E. Cha and L. P. Jin, *Cryst. Growth Des.*, 2012, **12**, 5227-5232.

41 Z. Dou, J. Yu, H. Xu, Y. Cui, Y. Yang and G. Qian, *Microporous Mesoporous Mater.*, 2013, **179**, 198-204.

42 Y. Cui, Y. Yue, G. Qian and B. Chen, *Chem. Rev.*, 2012, **112**, 1126-1162.

43 C. H. Zeng, F. L. Zhao, Y. Y. Yang, M. Y. Xie, X. M. Ding, D. J. Hou and S. W. Ng, *Dalton Trans.*, 2013, **42**, 2052-2061.

44 B. L. Chen, Y. Yang, F. Zapata, G. N. Lin, G. D. Qian and E. B. Lobkovsky, *Adv. Mater.*, 2007, **19**, 1693-1696.

45 D. Ma, W. Wang, Y. Li, J. Li, C. Daiguebonne, G. Calvez and O. Guillou, *CrystEngComm*, 2010, **12**, 4372-4377.

46 K. Chen, D. P. Dong, Z. G. Sun, C. Q. Jiao, C. Li, C. L. Wang, Y. Y. Zhu, Y. Zhao, J. Zhu, S. H. Sun, M. J. Zheng, H. Tian and W. Chu, *Dalton Trans.*, 2012, **41**, 10948-10956.

47 J. M. Zhou, W. Shi, H. M. Li, H. Li and P. Cheng, *J. Phys. Chem. C*, 2014, **118**, 416-426.

48 H. Li, W. Shi, K. Zhao, Z. Niu and P. Cheng, *Chem. Eur. J.*, 2013, **19**, 3358-3365.